Opto-electronic Zernike filter for high-resolution wavefront analysis using a phase-only liquid crystal spatial light modulator

Gary W. Carhart[a], Mikhail A. Vorontsov[a], and Eric W. Justh[b]

[a]Intelligent Optics Laboratory, U.S. Army Research Laboratory, Adelphi, MD 20783
[b]Institute for Systems Research, University of Maryland, College Park, MD 20742

ABTRACT

An opto-electronic technique for high-resolution wave-front phase imaging is presented and demonstrated experimentally. The technique is analogous to the conventional Zernike phase-contrast approach, but uses modern spatial light modulator technology to increase robustness and improve performance. Because they provide direct measurements of wave-front phase (rather than wave-front slope measurements, as in Shack-Hartmann sensors), robust phase-contrast sensors have potential applications in high-speed, high-resolution adaptive optic systems. Advantages of the opto-electronic approach over alternative advanced phase-contrast techniques (such as a related phase-contrast sensor which uses a liquid-crystal light valve exhibiting a Kerr-type optical response to perform Fourier filtering) are discussed. The SLM used for the experimental results is a 128×128-element pixilated phase-only liquid crystal spatial light modulator from Boulder Nonlinear Systems, Inc.

Keywords: wavefront sensor, phase visualization, Zernike filter, phase contrast microscopy, adaptive optics

1. INTRODUCTION

The emergence of high-speed, high-resolution optical wave-front shaping devices can have a significant impact in adaptive optics by enabling the design of compact, high-performance optical phase imagers: opto-electronic systems which can measure wave-front phase with resolution and speed that are currently only available in intensity imagers.[1,2] The key requirement of the optical part of the system is to provide an image with sufficient contrast that can be further transformed by electronic processing, using highly parallel algorithms, into a phase measurement of sufficient fidelity. The need for parallelism in the electronic processing is driven by the simultaneous requirements of high speed and high resolution. For example, Shack-Hartmann sensors, lateral shearing interferometers, and curvature sensors, in which the wave-front is numerically reconstructed from measurements of its spatial derivatives, are limited by time-consuming wave-front reconstruction calculations.

One way to use a high-resolution spatial light modulator (SLM) in a phase imaging system is by drawing an analogy with conventional phase-contrast techniques, such as the Zernike filter.[3,4] The Zernike filter uses a Zernike phase plate (consisting of a phase-shifting dot centered on a glass slide) between two lenses to phase-shift the zero-order Fourier component of the input beam (ideally, by $\pi/2$) relative to the rest of the Fourier spectrum. The superposition of the phase-shifted zero-order component with the rest of the beam produces an intensity pattern that is directly related to the input beam wave-front phase. Frits (Frederik) Zernike was awarded the 1953 Nobel Prize in physics for demonstrating the phase contrast technique and inventing the phase-contrast microscope (which is used in biology and medicine to visualize optical path-length differences produced by transparent specimens). Using an optically or electronically controlled phase SLM rather than the fixed Zernike phase plate can increase the robustness of the phase-contrast sensor. Since phase-contrast sensors can produce images that are directly related to input beam phase (rather than its derivatives), wave-front reconstruction calculations from the phase-contrast sensor image can use highly parallel algorithms. It is also possible to avoid numerical wave-front reconstruction altogether with such sensors, and instead use the dynamics of a parallel, distributed feedback system (adaptive optic system) to obtain a precise phase measurement (or perform wave-front phase distortion suppression).[1,2]

That an optically-controlled phase SLM could be used in place of the Zernike phase plate was suggested by Ivanov, et. al.[5] We refer to such wave-front sensors as advanced phase-contrast sensors. The idea was to use a Kerr slice (in which the index of refraction depends on optical intensity) or a liquid-crystal light valve (which exhibits a Kerr-type response at reasonable optical power levels) to produce a phase-shift for input wave spectral components with high intensity.[6] The resulting phase-contrast sensor is called the nonlinear Zernike filter because of the nonlinear (i.e., intensity-based) filtering operation in the Fourier domain.[1,2] If the phase aberrations in the input beam are small, so that most of the power is in the zero-order Fourier

component, the Kerr slice (or LCLV) will act like the Zernike phase plate and phase-shift the zero-order component. Unlike the conventional Zernike filter, this Kerr-slice sensor is robust to wave front tilts, because the peak-intensity Fourier component is the one phase-shifted regardless of where it falls on the Kerr slice (or LCLV).[1,2]

Although the nonlinear Zernike filter provides robustness to input beam wave-front tilts, a more general Fourier filtering operation would be possible with a more versatile, electronically-controlled SLM. This extra flexibility makes possible a better-performing opto-electronic phase-contrast wave-front sensor than the nonlinear Zernike filter: i.e., the differential Zernike filter.[1,2] Here we report on experimental results verifying the effectiveness of this novel opto-electronic Zernike filter for wave-front phase measurement. Section 2 discusses advanced phase-contrast sensors, their mathematical models, and how the mathematical models lead to the differential Zernike filter as a candidate high-performance phase-contrast sensor. Section 3 describes the experimental setup, and section 4 presents the experimental results. Finally, section 5 concludes by suggesting additional experimental work.

2. ADVANCED PHASE-CONTRAST SENSORS

2.1. Precise vs. imprecise phase measurement

An advanced phase-contrast wave-front sensor (e.g., the nonlinear or opto-electronic Zernike filter) could either be used alone as an imprecise phase sensor, or could instead be incorporated into a larger system for precise phase measurement (or an adaptive-optic system for phase correction). For phase-contrast microscopy, an imprecise phase sensor is sufficient, because the purpose of such a sensor is merely to obtain an image, with as high contrast as possible, of the specimen. Since the microscopist is only concerned about the shapes of features and not with measuring the actual index of refraction variations of different regions, there is no need to precisely measure the optical phase of the light passing through the sample.

However, if precise phase measurement is required, then the imprecise phase sensor must be augmented either with electronic processing to reconstruct the phase from the sensor image, or else the imprecise phase sensor can be incorporated into a feedback system which converges to a precise phase measurement through an iterative process.[1,2] We are interested in phase sensors which are compatible with precise phase measurement, which narrows the phase-contrast sensor candidates we consider. For example, the Smartt point-diffraction interferometer produces a high-contrast image suitable for imprecise phase measurement, but its output is unsuitable for a parallel, distributed wave-front reconstruction algorithm (at least for small-amplitude phase variations), or for incorporating into a parallel, distributed feedback system.[1,2] (The point-diffraction interferometer resembles the conventional Zernike filter, but with the transparent phase-shifting dot on the Zernike phase plate replaced by an opaque dot to block the zero-order Fourier component.[7] The resulting sensor output is not proportional to input beam wave-front phase for small phase variations.) Instead, we consider the differential Zernike filter, which has higher contrast than the conventional Zernike filter, but does provide an output image suitable for precise phase measurement. The tradeoff is that the differential Zernike filter entails greater complication from an engineering standpoint to realize.

Whereas the idea for the conventional Zernike filter arose more than six decades ago from the physics question of how to make optical phase visible, the idea for the differential Zernike filter arose within the past couple of years from a theoretical analysis of how best to measure optical phase for purposes of direct feedback control.[1,2]

2.2. Ideal opto-electronic Zernike filter model

The output intensity distribution resulting from the conventional Zernike wave-front sensor can be obtained analytically. For a $\pi/2$ phase shift of the zero-order component of the spectrum, this output intensity distribution is given by the expression

$$I_{out}(\boldsymbol{r}) = I_0(\boldsymbol{r}) + 2(2\pi F)^2 I_F(0) - 4\pi F \sqrt{I_0(\boldsymbol{r})I_F(0)} \left\{ \cos[\varphi(\boldsymbol{r}) - \Delta] - \sin[\varphi(\boldsymbol{r}) - \Delta] \right\} \qquad (1)$$

where $\boldsymbol{r}$ is a coordinate vector in the input or output planes, $I_0(\boldsymbol{r})$ and $\varphi(\boldsymbol{r})$ are the intensity and phase distributions in the input plane, F is the focal length of the Fourier lens, $I_F(0)$ is the intensity of the zero-order component in the focal plane and Δ is a phase constant.[1] To obtain the above expression it is assumed that the input wave field does not contain any mean tilt so that the zero-order component of the spectrum will indeed be located at the origin in the focal plane. The intensity distribution (1) has a term that is proportional the phase of the input wave field. There are three problems involved in using this technique to develop a wavefront sensor for adaptive optics applications. First, the presence of wave-front tilts dynamically changes

location of the DC component of the spectrum. This implies a Zernike wave-front sensor will require a "movable" phase spot. Next, the intensity distribution in the output plane is a function of phase modulation and any intensity modulation in the input plane. Separating the desired phase related component from the remainder of the intensity modulation must be accomplished. Finally, the mapping from detected intensity in the output plane to phase requires the use of a time-consuming phase "unwrapping" technique.

Moving the phase spot in response to input beam wave-front tilts is accomplished in the nonlinear Zernike filter, and can be readily accomplished with an opto-electronic Zernike filter, as well. However, if the input beam has intensity modulation, the nonlinear Zernike filter has the same problem as the conventional Zernike filter with the sensor output being influenced by both the intensity modulation and phase modulation of the input beam. The differential Zernike filter has much better properties in the presence of input beam intensity modulation.[1,2] The differential Zernike wave-front sensor output intensity distribution is the difference of the output intensity distributions produced by alternately applying phase shifts of $\pi/2$ and $-\pi/2$ to the input field zero-order spectral component. Labeling these two intensity distributions $I_{zer}^{(+)}(\boldsymbol{r})$ and $I_{zer}^{(-)}(\boldsymbol{r})$, where $I_{zer}^{(+)}(\boldsymbol{r}) = I_{out}(\boldsymbol{r})$ of equation (1), we have

$$I_{out}(\boldsymbol{r}) \equiv I_{zer}^{(-)}(\boldsymbol{r}) = I_0(\boldsymbol{r}) + 2(2\pi F)^2 I_F(0) - 4\pi F \sqrt{I_0(\boldsymbol{r})I_F(0)}\left\{\cos[\varphi(\boldsymbol{r}) - \Delta] + \sin[\varphi(\boldsymbol{r}) - \Delta]\right\} \qquad (2)$$

and the difference between the intensity distributions (1) and (2) is then

$$I_{dif}(\boldsymbol{r}) \equiv I_{zer}^{(+)}(\boldsymbol{r}) - I_{zer}^{(-)}(\boldsymbol{r}) = 8\pi F \sqrt{I_0(\boldsymbol{r})I_F(0)}\,\sin[\varphi(\boldsymbol{r}) - \Delta]\,. \qquad (3)$$

Observe that the spatially uniform terms $I_0(\boldsymbol{r}) + 2(2\pi F)^2 I_F(0)$ have been cancelled by the subtraction, as well as the $4\pi F \sqrt{I_0(\boldsymbol{r})I_F(0)}\,\cos[\varphi(\boldsymbol{r}) - \Delta]$ term.

The differential Zernike filter eliminates an additive component related to the input beam intensity distribution, as can be seen by comparing equation (3) to equation (1). The $I_0(\boldsymbol{r})$ term could also have been eliminated in the conventional or nonlinear Zernike filter by subtracting the input beam intensity distribution directly from the wave-front sensor output. However, the $2(2\pi F)^2 I_F(0)$ term would remain, and this spatially uniform term (which is proportional to the Strehl ratio, and so depends on the degree of phase modulation) would also need to be estimated (or measured) and subtracted from the sensor image before further processing to remove the effects of input beam intensity modulation.

The response of the differential Zernike filter is seen from equation (3) to be a sinusoidal function of the phase distribution of the input beam, modulated by the square-root of the intensity distribution of the input beam. Therefore, all that is necessary to separate the phase-modulation contribution from the intensity-modulation contribution to the sensor output image is to divide the sensor output by the square root of the input beam intensity distribution. If the differential Zernike filter is incorporated into a feedback system for phase distortion suppression, the dynamics of the feedback system can automatically compensate for the intensity-modulation effect in the sensor response, so dividing by the square root of the input beam intensity distribution is not even necessary for that application.[1,2] Similar remarks apply for the terms Δ and $I_F(0)$ in equations (1)-(3), which are both spatially uniform, but depend on the input beam phase profile. A feedback system can drive these terms to their nominal values for an unaberrated beam (i.e., $\Delta = 0$ and $I_F(0) = I_F^0$, the intensity of the zero-order component of an unaberrated beam). Otherwise, in principle, Δ and $I_F(0)$ should be calculated from the wave-front sensor image and information available from the Fourier-domain image used to control the Fourier-domain filter.

From the sinusoidal dependence of the differential Zernike filter response on input beam wave-front phase given by equation (3), we see that there will be phase ambiguity if the phase modulation exceeds π radians. Using the differential Zernike filter in a feedback system can allow phase modulation up to 2π radians without ambiguity.[1,2] Resolving these phase ambiguities at the same high speed as the wave-front sensing remains an open problem.
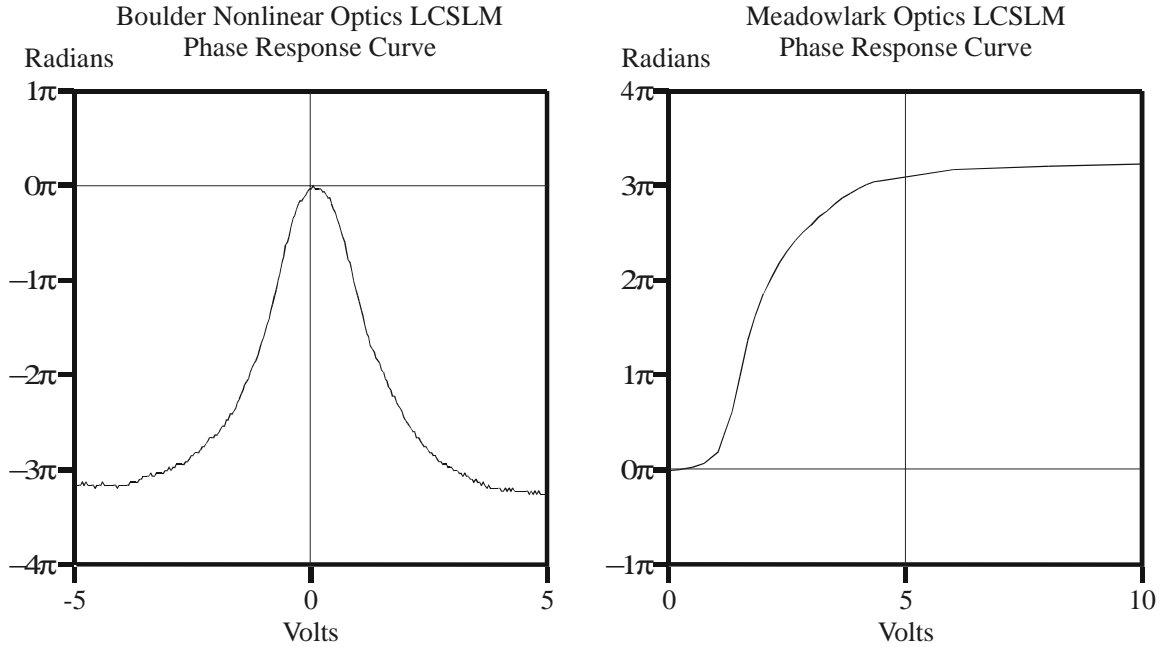
Figure 1: Phase response to drive voltage of the two LC phase SLMs used in the Zernike phase contrast wavefront sensor experimental setup. The zero phase shift reference in the plots corresponds to the constant phase shift produced by either device when there is no drive voltage.
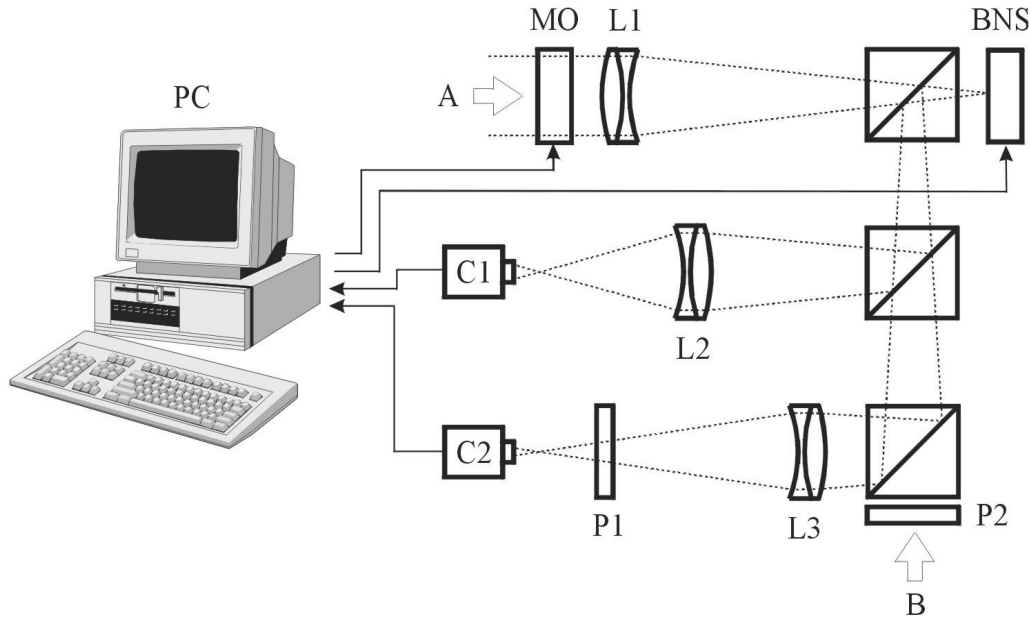
3. EXPERIMENTAL SETUP

High-resolution pixilated phase-only liquid crystal spatial light modulators (LC SLMs) capable of performing the Fourier-domain filtering are currently available from several commercial vendors. To determine which SLM pixels to phase shift, an additional optical system should be included that images the intensity distribution in the focal plane (the Fourier spectrum) and obtains the coordinates of the zero-order spectral component (presumably the peak spectral intensity pixel, centroid of the spectral intensity distribution, or something similar).

To implement a laboratory prototype of an opto-electronic Zernike wave-front sensor we used a 128×128 phase-only LC SLM manufactured by Bolder Nonlinear Systems, Inc. (BNS) as the Zernike phase shifting element.[8] This device can update the phase pattern at the rate of 200 Hz and can provide a phase shift of zero to 3π radians individually at each pixel. The pixel pitch is 40 microns, and the fill factor is 60%. The fill factor is important because the regions between the active pixel areas introduce parasitic Fourier-domain filtering, which affects the sensor output image. The LC SLM has a LC layer placed on top of an array of electrodes, which define the active pixel areas. While the phase shift due to the LC layer interpolates somewhat between the active pixel regions, the reflectivity varies between the active pixel areas and the inter-pixel gaps. With more recent LC SLMs achieving an 80% fill factor, this parasitic filtering should be less of a problem for these SLMs. It is encouraging that good results were obtained even for the device with a 60% fill factor.

Figure 1 (left) shows the response curve of the BNS LC SLM device. The symmetric shape of the response curve is the result of the mapping from eight bit digital values to drive voltages used in the digital interface controlling the device. Zero volts (which produces maximum retardation) is located in the middle of the range of eight bit values and only the absolute value of a drive voltage determines the device phase response. To calibrate the obtained intensity response of the system to the phase of the input wave field, a source of known phase distortions is required. For this purpose we used a Meadowlark Optics HEX127 phase-only LC SLM. The HEX127 contains 127 individually addressed hexagonal LC cells. Figure 1 (right) shows the response curve of the Meadowlark LC SLM. As can be seen in the response curves, both devices can only be regarded as linear over a limited range of the control voltages.

Figure 2 shows a schematic of our optical system that implements a Zernike wave-front sensor. The HEX127 LC SLM is located in the system input plane (labeled MO in the Figure). The HEX127 device modulates the phase of the input wave

Figure 2: Schematic of the experimental setup implementing the Zernike wavefront sensor

(labeled A in the Figure). Lens L1 produces the Fourier transform of the input wave field. The BNS LC SLM is located in the lens focal plane (labeled BNS in the Figure). It changes the phase of the input wave spectral components inside a programmable area. The system output is obtained by camera C1 after lens L2 reconstructs the filtered Fourier transform. To obtain the information required to keep the $\pi/2$ phase shift at the location of the DC component of the spectrum, lens L3 images the surface of the BNS LC SLM at camera C2. Centering and scaling adjustments are accomplished by illuminating the BNS device with incoherent light (labeled B in the Figure) and using crossed polarizers (P1 and P2) oriented at 45 degrees relative to the LC SLM director to capture an intensity response with camera C2. With this arrangement both the spatial spectrum of the input wave and the phase pattern placed on the BNS device are visible simultaneously, permitting easy adjustment. Translation and scaling information is required to relate the image captured by camera C2 to the phase pattern to be placed on the LC SLM. Centering with mechanical translation is accomplished easily, but scaling can only be accomplished optically if the aspect ratio of the active area of the LC SLM is the same as the CCD chip area of camera C2. As this was not the case in our optical system, scaling had to be accomplished numerically with a computer. A Dell Dimension XPS R400 desktop computer running Windows NT was used to control the system, perform the scaling transformation, and automate data collection.

4. EXPERIMENTAL RESULTS

We used the experimental system to measure the response of the differential Zernike filter for various sizes of the phase-shifted spot. A baseline phase shift of π was first applied to all of the SLM pixels, and the $\pi/2$ and $-\pi/2$ phase shifts were with respect to that baseline phase value. Figure 3 shows typical output intensity distributions for the two steps in the differential Zernike filtering process and the final output result. Also shown is a gray level pattern of the phase shifts on the HEX127 device that produced the resulting output intensity. As can been seen, there is good correlation between these two patterns. To both calibrate the response and obtain a quantitative assessment of the performance of the system, we collected 1000 output images generated using uniformly distributed random input voltages in the range one to five volts on the HEX127 LC SLM. To get the output intensity response associated with a known input voltage, the intensity distribution within the region of the output image corresponding to each Meadowlark pixel was averaged. Each input-voltage/output-intensity-response pair was then added into a two-dimensional histogram. Since the HEX127 device has 127 pixels, the histogram was built from 127000 input and response pair samples. The information in the histogram was then used to compute the mean intensity response to each input voltage.
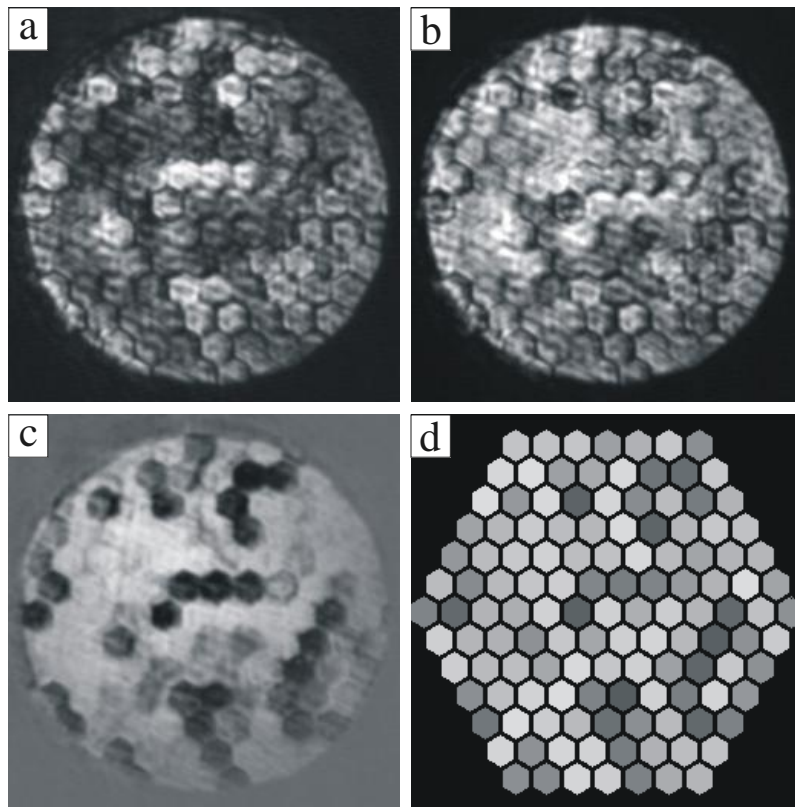
Figure 3: Detecting phase with the differential Zernike filtering process. (a) Intensity output obtained after shifting the input field spectrum DC component by $+\pi/2$ radians. (b) Intensity output obtained after shifting the input field spectrum DC component by $-\pi/2$ radians. (c) Final output obtained after subtracting image (a) from image (b). (d) The actual phase distribution present at the input plane (gray levels correspond to phase shifts from zero to $\pi/2$ radians).

Figure 4 shows an example of one such histogram, corresponding to a phase-shift spot radius of 3 pixels. The horizontal axis is the Meadowlark Optics SLM pixel voltage, which corresponds to optical phase shift through figure 1 (right), and the vertical axis corresponds to output image gray-level. Figure 4 shows that the data is clustered around a clearly-defined mean curve, and also gives an idea of the extent of deviation from the mean curve. Two types of factors can account for the observed deviation from the mean curve: those associated with limitations in the experimental setup, and those inherent to this type of phase-contrast sensor measurement. The former category includes effects such as deviation of individual Meadowlark Optics SLM pixel responses from the nominal curve shown in figure 1 (right), parasitic Fourier filtering due to the limited fill factor of the LC SLM, nonuniformity of the input beam intensity distribution, mechanical vibrations in the system, etc. Effects inherent to the phase-contrast sensor measurement are those indicated by equation (3), and no attempt is made to numerically correct for any of these effects through sensor image post-processing. For example, the extent of the phase distortion impacts $I_F(0)$, the intensity of the zero-order Fourier component, which affects the overall scaling of the wave-front sensor output image. The value of Δ can also vary from one Meadowlark Optics SLM phase image to the next, since Δ depends on the particular phase profile of the input beam.[1]

We also investigated what filter radius will be optimal (in the sense of maximizing the visibility of the output intensity distribution) by collecting 5 histograms such as Figure 4, but with different filter radii. The mean detected output responses from this data set are shown in Figure 5. Using the HEX127 phase-response-to-drive-voltage curve (Figure 1, right) and these mean output intensity responses to input voltage, the system output intensity response to input phase can be obtained. Figure 5 shows the mean curves as a function of Meadowlark Optics SLM voltage, and figure 6 shows them as a function of input beam phase. Presumably the single pixel filter case (filter radius equals one) is the closest approximation to the true sinusoidal response expected from the analytical expression, but it obviously does not produce the best visibility. The visibilities computed from the five curves in Figure 6 are shown in Figure 7, and reveal that the Zernike filter output visibility

Figure 4: The distribution of output intensity responses to input voltages. The vertical axis of the picture is detected output intensity. The third axis (gray level of the points in the picture) is the number of occurrences of each input voltage output intensity pair.

is maximized for a spot radius equal to four. This optimum size is of course a function of the size of the Fourier transform in the focal plane, and so is specific to this system. An approximate calculation for the size of the zero-order component is

$$b = 1.22\lambda F / a = 1.22(.514)(1.5) / .0127 \,\mu m = 74 \mu m, \tag{4}$$

where λ is the wavelength, F is the focal length of the Fourier transforming lens, a is the diameter of the beam aperature, and b is the diameter of the central lobe in the Fourier plane (for an unaberrated input beam with uniform intensity over the aperature of diameter a). In practice, the spot size in the Fourier plane is somewhat larger than the value given by equation (4), due to aberrations in optical components. Given the 40μm pixel pitch of the SLM, this calculation is in general agreement with the experimental data of figures 6 and 7 showing high-contrast phase measurement corresponding to an SLM phase-shift region radius of 3 to 5 pixels.

5. CONCLUSIONS

We have presented preliminary experimental results for an advanced phase-contrast sensor capable of overcoming some of the limitations of conventional phase-contrast sensors, and which is suitable for high-speed, high-resolution wave-front phase measurement. Such a sensor could be used by itself for imprecise phase visualization (e.g., in a phase-contrast microscope), or could be supplemented with additional electronic processing to produce a higher-fidelity phase image. Such a sensor could also be used to augment a conventional adaptive optic system, or could be used in a parallel, distributed feedback system for precise phase measurement or for phase distortion suppression.

The same basic experimental setup used to obtain the results reported here can also be used to investigate other possibilities for the Fourier filtering operation (besides simply phase-shifting the zero-order component by $\pi/2$ and $-\pi/2$). Examples include differential versions of the nonlinear Zernike filter function (i.e., alternating positive and negative phase shifts corresponding to the Fourier-domain intensity distribution), or using a Gaussian phase-shifting spot rather than a step-function. Smoothing the Fourier-domain intensity distribution may improve sensor performance, and could potentially be implemented in analog electronic circuitry integrated with the imaging array.[9]

Several issues remain to be investigated which could influence the ultimate choice of the Fourier filtering operation to use with the differential Zernike filter. For a highly aberrated input beam, the location of the zero-order component may be ambiguous. One possibility would be to use the centroid of the Fourier intensity distribution as a measurement of the location of the zero-order component. It is not clear that only using the centroid is good enough, because if the beam is highly aberrated, too little of the power may be phase-shifted if the Fourier filter phase-shifts only the Fourier component corresponding to the centroid. If additional information, such as a beam-quality metric related to the moments of the Fourier intensity distribution about the centroid, were available, then that information could potentially be used to control the spot

Mean Gray Level
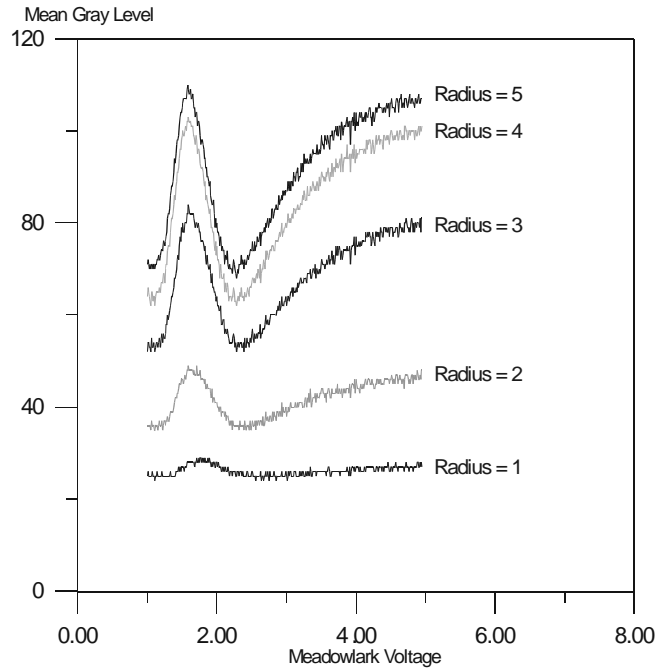
Figure 5: Mean detected output intensity vs. Meadowlark input voltage for 5 different cases of the size of the Zernike filter DC shifting spot.

Output Gray Level
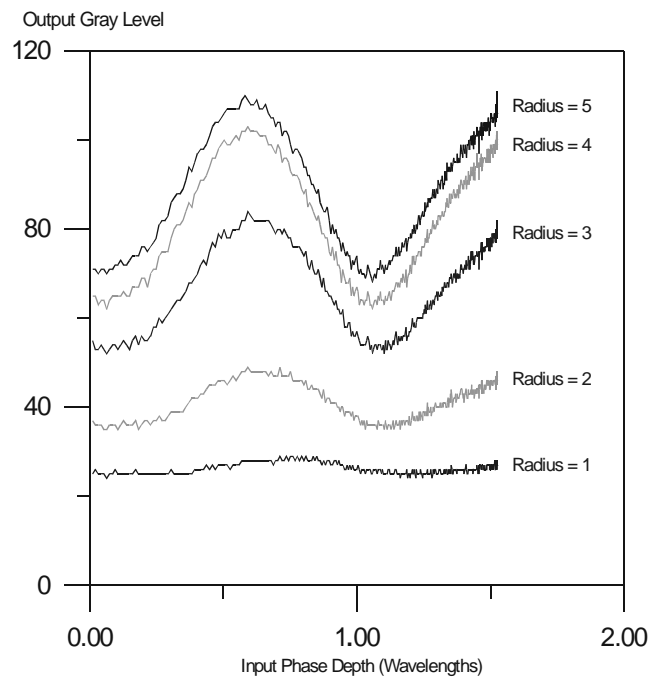
Figure 6: Intensity output vs. input phase for 5 different cases of the size of the Zernike filter DC shifting spot.

size in order to phase shift closer to half of the input beam power. However, increasing the spot size affects the phase image, so there may be a tradeoff between accuracy and image contrast. There also may be computational tradeoffs: the optimal

Output Graylevel Visibility
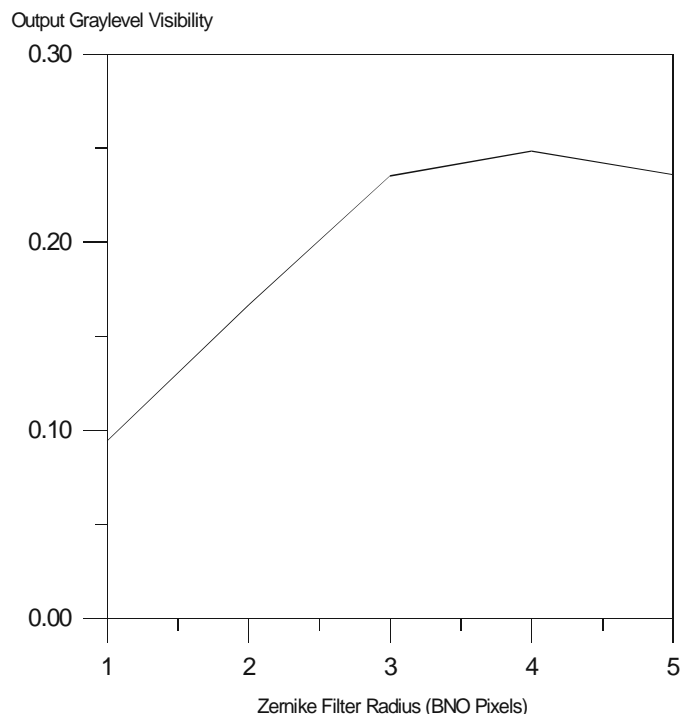
Figure 7: Dependence of output intensity visibility on the radius of the Zernike filter DC shifting spot.

choice of Fourier-intensity-to-Fourier-phase-shift mapping may be difficult to compute fast enough for high-speed phase imaging, so a more readily computed approximation may be more appropriate.

Another issue is the role of SLM pixel size with respect to zero-order component size, and in particular, how the limited fill-factor impacts the optimal ratio of pixel size to zero-order component size. For each of these questions, experimental investigation is quite useful, because not all of the effects important for the actual system are easily incorporated into simulations. The experimental work done so far illustrates the merit of the basic concept, and motivates further investigation to answer these other questions.

ACKNOWLEDGEMENTS

REFERENCES

1. M. A. Vorontsov, E. W. Justh, and L. Beresnev, "Adaptive Optics with Advanced Phase-Contrast Techniques: Part I. High-Resolution Wavefront Sensing," submitted to *J. Opt. Soc. Am. A*, 2000.
2. E. W. Justh, M. A. Vorontsov, G. W. Carhart, L. Beresnev, and P. S. Krishnaprasad, "Adaptive Optics with Advanced Phase-Contrast Techniques: Part II. High-Resolution Wavefront Control," submitted to *J. Opt. Soc. Am. A*, 2000.
3. F. Zernike, "How I Discovered Phase Contrast," *Science*, **121**, 345-349 (1955).
4. J.W. Goodman, "*Introduction to Fourier Optics*," McGraw-Hill (1996).
5. V.Yu. Ivanov, V.P. Sivokon, and M.A. Vorontsov, "Phase retrieval from a set of intensity measurements: theory and experiment," *J. Opt. Soc. Am.*, **9**(9), 1515-1524 (1992).
6. S.A. Akhmanov and S. Yu. Nikitin, "*Physical Optics*," Clarendon Press, Oxford (1997).

7. R.N. Smartt, and W.H. Steel, "Theory and application of point-diffraction interferometers, *Japanese Journal of Applied Physics*, 272-278 (1975).

8. S. Serati, G. Sharp, R. Serati, D. McKnight and J. Stookley, "128x128 analog liquid crystal spatial light modulator," *SPIE*, **2490**, 55 (1995).

9. V. Gruev and R. Etienne-Cummings, "A Programmable Spatiotemporal Image Processor Chip," *Proc. IEEE International Symposium on Circuits and Systems*, vol. 4, pp. 325-328, (2000).